



Coordination of contractile tension and cell area changes in an epithelial cell monolayerAashrith Saraswathibhatla ¹, Jun Zhang ^{1,2} and Jacob Knotbohm ^{1,2,*}¹*Department of Engineering Physics, University of Wisconsin-Madison, Madison, Wisconsin 53706, USA*²*Biophysics Program, University of Wisconsin-Madison, Madison, Wisconsin 53706, USA*

(Received 7 October 2021; revised 14 January 2022; accepted 1 February 2022; published 17 February 2022)

During tissue development and repair, cells contract and expand in coordination with their neighbors, giving rise to tissue deformations that occur on length scales far larger than that of a single cell. The biophysical mechanisms by which the contractile forces of each cell cause deformations on multicellular length scales are not fully clear. To investigate this question, we began with the principle of force equilibrium, which dictates a balance of tensile forces between neighboring cells. Based on this principle, we hypothesized that coordinated changes in cell area result from tension transmitted across the cell layer. To test this hypothesis, spatial correlations of both contractile tension and the divergence of cell velocities were measured as readouts of coordinated contractility and collective area changes, respectively. Experiments were designed to alter the spatial correlation of contractile tension using three different methods, including disrupting cell-cell adhesions, modulating the alignment of actomyosin stress fibers between neighboring cells, and changing the size of the cell monolayer. In all experiments, the spatial correlations of both tension and divergence increased or decreased together, in agreement with our hypothesis. To relate our findings to the intracellular mechanism connecting changes in cell area to contractile tension, we disrupted activation of extracellular signal-regulated kinase (ERK), which is known to mediate the intracellular relationship between cell area and contraction. Consistent with prior knowledge, a temporal cross-correlation between cell area and tension revealed that ERK was responsible for a proportional relationship between cell area and contraction. Inhibition of ERK activation reduced the spatial correlations of the divergence of cell velocity but not of tension. Together, our findings suggest that coordination of cell contraction and expansion requires transfer of cell tension over space and ERK-mediated coordination between cell area and contraction in time.

DOI: [10.1103/PhysRevE.105.024404](https://doi.org/10.1103/PhysRevE.105.024404)**I. INTRODUCTION**

In various processes in tissue development and repair, epithelial cells undergo large changes in area, giving rise to global tissue deformation [1–3]. For example, in healing of small circular wounds, cells at the wound edge collectively stretch in the radial direction as the wound closes [4,5]. Similarly, in the common *in vitro* scratch wound assay, the expansion of cells into free space depends more so on cell migration than proliferation [6,7], indicating that the cells must stretch to increase their spread area. In cell monolayers, changes in cell area are typically far larger than changes in cell height, meaning that fluctuations in area are associated with fluctuations in cell volume [8]. Cell area changes are often spatially correlated over 10 or more cell lengths [9,10]. Hence, cells coordinate with their neighbors to contract and expand in collective groups of characteristic size. This observation is intriguing, because a large group of collectively contracting cells requires large motion of cells at the edges of the group. It would seem that a more favorable situation would be one in which a cell's contraction is anticorrelated with that of its neighbor, which would allow the monolayer to remain confluent while minimizing the need for larger

scale collective motion. Nevertheless, contraction is indeed correlated between neighbors, indicating that there must be some biophysical mechanism that coordinates the contraction over space.

From a physical perspective, contraction of a cell results from a change in the balance of physical forces within the cell layer. At the level of a single cell, *in vitro* experiments in cell monolayers have shown that force and area are related through the extracellular signal-regulated kinase (ERK) pathway. When a cell's area is increased, ERK is activated, which triggers cell contractility through Rho signaling, in turn causing the cell's area to decrease [11–13]. The ERK-mediated feedback between cell stretching and contractile forces can produce interesting biomechanical phenomena, including waves of activated ERK, contractile tension, and collective motion that propagate across the cell layer [12–17]. Such waves of ERK activity, force production, and cell motion occur *in vivo* as well, and they are important for epithelial invagination in the developing *Drosophila* embryo [18] and for regeneration of zebrafish scales [19]. Intriguingly, even though the ERK-mediated relationship between cell area and contraction exists within each cell, images of ERK activation indicate that ERK activity is spatially correlated over ≈ 6 –8 cell lengths [12,13,17,18]. Similarly, experiments and modeling suggest that phosphorylated myosin light chain is spatially correlated over similar length scales [20,21]. Although the

*jknotbohm@wisc.edu

causes of these spatial correlations are not fully clear, one important factor for spatial correlation of ERK is transmission of force by cell–cell adhesions [12]. In support of the importance of physical forces is that the principle of force equilibrium requires that stresses between neighboring cells be spatially correlated. Indeed, experimental data indicate that tensile stresses are typically correlated over a distance of ≈ 10 cell lengths [22–24], which is of similar size to the correlation length of changes in cell area and only slightly larger than the correlation length of ERK activation. Together, the prior research points to the hypothesis that tensile stress transmitted across the cell layer by force equilibrium controls the length scale of collective area changes in a cell monolayer, though this hypothesis has not been tested directly, because the prior studies focusing on ERK activity have not quantified tensile stresses experimentally.

Here, we investigated the roles of both tensile stresses and ERK activity in collective cell area changes in monolayers of Madin-Darby canine kidney (MDCK) epithelial cells. The local area change was quantified by the divergence of the cell velocity field, $\text{div}(\vec{v})$, and force transmission across the cell layer was quantified by the tensile stress. We designed experiments to perturb the transmission of stresses across the cell layer and to quantify the resulting effect on the correlation length of $\text{div}(\vec{v})$. Additionally, we investigated the role of ERK signaling on spatial correlations of both $\text{div}(\vec{v})$ and tensile stress.

II. MATERIALS AND METHODS

A. Cell culture

MDCK type II cells expressing green fluorescent protein (GFP) attached to a nuclear localization signal were obtained from the laboratory of Professor David Weitz, Harvard University. The cells were maintained in 1 mg/ml glucose Dulbecco’s modified Eagle’s medium (Cellgro 10-014-CV, Corning Inc., Corning, NY) with 10% fetal bovine serum (Corning) and 1% G418 (Corning) in an incubator at 37°C and 5% CO₂, and were passaged every 2–3 days until passage 20. For experiments that treated cells with EGTA and U0126, cells were maintained in 2% fetal bovine serum 6–8 h before the start of the experiments. In the experiments that treated the cells with CN03, a low concentration (1%) of serum was used, which was required to reduce the baseline levels of cell contractility. In these experiments, referred to in the text as low serum, medium was replaced with medium containing 1% serum 24 h before the start of the experiment.

B. Polyacrylamide substrates and micropatterning

Polyacrylamide substrates of Young’s modulus 6 kPa were fabricated and micropatterned as described previously [25]. Briefly, polyacrylamide substrates were fabricated to have fluorescent particles embedded at the top. Next, polydimethylsiloxane masks having holes of diameter 0.5, 1, 1.5, or 3 mm were placed on the gels. Most experiments used islands of diameter 1 mm; diameters of 0.5, 1.5, and 3 mm were used as described in the text. Collagen I (0.1 mg/ml) was crosslinked to the gels using sulfo-SANPAH. Cells were seeded at confluency 8–12 h before the start of the imaging. The masks

were removed within 2–3 h of cell seeding. For the 0.5 mm cell islands, fluorescent particles of 0.2 μm diameter were embedded in the polyacrylamide gels, whereas for 1, 1.5, and 3 mm islands, fluorescent particles of 0.5 μm diameter were used.

C. Time lapse imaging

Time lapse imaging of cells, GFP nuclei, and fluorescent particles was performed using an Eclipse Ti microscope (Nikon Instruments, Melville, NY) with a 10 \times numerical aperture 0.3 objective or a 20 \times numerical aperture 0.5 objective (Nikon) and an Orca Flash 4.0 camera (Hamamatsu, Bridgewater, NJ) controlled by Elements Ar software (Nikon). Cells were maintained at 37°C and 5% CO₂ using a custom-built cage incubator. Images were collected every 10 min. After the imaging, cells were removed by incubating in 0.05% trypsin for 40 min, and images of the fluorescent particles in the substrate were captured for a traction-free reference state to compute cell-substrate tractions.

D. Divergence of cell velocity

Cell velocities were measured using Fast Iterative Digital Image Correlation between consecutive time-lapse phase contrast images using 48×48 pixel ($31 \times 31 \mu\text{m}^2$) subsets at a spacing of 12 pixels (8 μm) [26]. The divergence of the velocity field $\text{div}(\vec{v})$ was computed using the divergence theorem, as done previously [9]. The divergence theorem for the velocity field \vec{v} in two dimensions is defined as

$$\int_{\Omega} \nabla \cdot \vec{v} dA = \int_{\partial\Omega} \vec{v} \cdot \hat{n} ds, \quad (1)$$

where Ω is an area over which the divergence is computed, $\partial\Omega$ is the boundary of Ω , \hat{n} is the unit vector normal to the boundary, and dA and ds are differential area and length elements. We were interested in the average divergence over Ω , which simplified the left-hand side of Eq. (1) to $\Omega \text{div}(\vec{v})$. Additionally, we used a circular area for Ω , in which case the integrand of the right-hand side of Eq. (1) simplified to the radial component of velocity v_r . With these simplifications, the divergence was computed according to

$$\text{div}(\vec{v}) = \frac{1}{\Omega} \int_{\partial\Omega} v_r ds. \quad (2)$$

Before computing $\text{div}(\vec{v})$, the velocity field was averaged over 2 h to smooth out high frequency fluctuations. To compute $\text{div}(\vec{v})$, the circular area Ω had a radius of 25 μm . The divergence was computed on each grid point for which velocity was obtained by image correlation.

E. Traction force microscopy and monolayer stress microscopy

Cell-induced substrate displacements were measured using Fast Iterative Digital Image Correlation [26] using 32×32 pixel ($21 \times 21 \mu\text{m}^2$) subsets centered on a grid with spacing of 8 pixels (5.2 μm). Cell-substrate tractions were computed using unconstrained Fourier transform traction microscopy [27] accounting for the finite substrate thickness [28,29]. Cell-cell stresses were computed using monolayer stress microscopy, which applies the principle of force equilibrium between the

cell-substrate tractions and the cell-cell stresses [22,30]. The code used for monolayer stress microscopy is available online [31] with a sample set of data [32]. Monolayer stress microscopy computes the three independent components of the in-plane stress tensor; here we analyzed the mean principal stress, which we refer to as the tension. To match the spatial resolution of $\text{div}(\bar{v})$ ($25 \mu\text{m}$), the tension measured at each grid point was spatially averaged in a circle of radius $25 \mu\text{m}$ centered at that grid point, and data points near the boundary of the cell layer (i.e., within $50 \mu\text{m}$ of the boundary) were excluded.

F. Spatial correlation

The spatial correlation C_s of a scalar variable u was measured according to

$$C_s(r') = \frac{\sum \bar{u}(\bar{r})\bar{u}(\bar{r} + \bar{r}')}{\sum \bar{u}^2}, \quad (3)$$

where $\bar{u} = u - u_m$ with u_m being the mean of u , \bar{r} and \bar{r}' are position vectors, the sum is over all starting positions \bar{r} , and the results are averaged for all cells separated a distance $r' = |\bar{r}'|$.

G. Temporal cross-correlation of cell area and contractile tension

To compute a temporal cross-correlation between cell area and tension, we first mapped area and tension to each cell. To this end, cell nuclei were segmented from images of the GFP-labeled nuclei using the ImageJ plugin StarDist [33]. To compute cell trajectories, we tracked cell nuclei as described previously [34]. Briefly, each nucleus center was identified from segmented images at each time point, and each center was mapped to the nearest cell nucleus at the next time point using the `knnsearch` function in Matlab, allowing for cell trajectories and velocities to be computed. To measure areas of individual cells in a monolayer, we approximated cell outlines from a Voronoi tessellation built from the centers of the cell nuclei [35]. To measure single cell contractile tension, the field of contractile tension was mapped onto each Voronoi-based polygon, and an average of the tension data in each polygon was computed. Cell areas and tensions were tracked over time using the data identifying each cell's trajectory.

The temporal cross-correlation C_t was computed on the single cell areas A and tensions T according to

$$C_t(t') = \frac{\sum \bar{A}(t)\bar{T}(t + t')}{\sqrt{\sum_t \bar{A}^2} \sqrt{\sum_t \bar{T}^2}}, \quad (4)$$

where $\bar{A} = A - A_m$ and $\bar{T} = T - T_m$ with A_m and T_m being the means of A and T , t and t' are time points, the sum is over all starting time points t , and the results are averaged for all time points separated by t' .

H. Chemical treatments

The chemical treatments used were EGTA (Sigma-Aldrich, Inc., St. Louis, MO), U0126 (Sigma-Aldrich), and CN03 (Cytoskeleton, Inc., Denver, CO). The stock solution of EGTA was prepared at 100 mM in deionized water that was verified

to have a pH of 7. The stock solution of U0126 was prepared at 20 mM in dimethyl sulfoxide. The stock solution of CN03 was prepared in deionized water at 0.1 g/l. The stock solutions were diluted in phosphate-buffered saline to obtain the desired concentrations for the experiments.

I. Cell velocity alignment

To calculate alignment of velocity between neighboring cells, we computed the dot product of each cell's velocity with that of all of its neighbors within a radius of $25 \mu\text{m}$ (which is slightly larger than the typical cell size of $\approx 20 \mu\text{m}$), and took the mean of the dot products. To compute the alignment for each island, we averaged the dot products over all the cells in the island.

J. Immunofluorescence and confocal imaging

For imaging of stress fibers, cells were rinsed twice with phosphate-buffered saline and fixed with 4% formaldehyde for 20 min. The cells were then washed with Tris-buffered saline twice for 5 min and incubated in 0.1% Triton X-100 for 5 min at room temperature. To stain for F-actin, the cells were treated with 3–5 units/ml Phalloidin Dylight 594 (catalog no. 21836, Thermo Fisher Scientific, Waltham, MA). For staining of phosphorylated ERK (pERK), cells were treated with phospho-p44/42 MAPK (ERK1/2) primary antibody (1:200 ratio, catalog no. 9101S, Cell Signaling, Danvers, MA). After washing the cells, Alexa 647 antirabbit antibody (1:400 ratio, Catalog No. A-21245, Thermo Fisher) was used for fluorescent staining of the primary antibody. Fluorescent images of stress fibers and pERK were captured using an AIR+ confocal microscope with a $40\times$ numerical aperture 1.15 water-immersion objective using Nikon Elements Ar software.

K. pERK analysis

The spatial correlation of pERK intensity was computed based on the intensity of the original image (without median subtraction) following Eq. (3).

L. Statistical tests

Statistical comparisons were performed using a two-sided Student's t -test between two groups, and, for more than two groups, one-way analysis of variance using Tukey's correction for multiple comparisons. A value of $p < 0.05$ was considered statistically significant.

III. RESULTS

We began with MDCK cell monolayers confined in circular islands of 1 mm diameter [Fig. 1(a)] at an initial cell density of ≈ 2500 cells/mm² [Fig. S1(a)] [37] and performed time-lapse microscopy by phase contrast imaging (Video 1) [37]. Over 3 h of imaging, cell areas changed, with some decreasing and others increasing. As the imaging was by phase contrast, the area changes apparent in the images represent changes in the average area through the height of each cell, and given that changes in height are far smaller than changes in area for this cell type [8], these area changes coincided with changes in

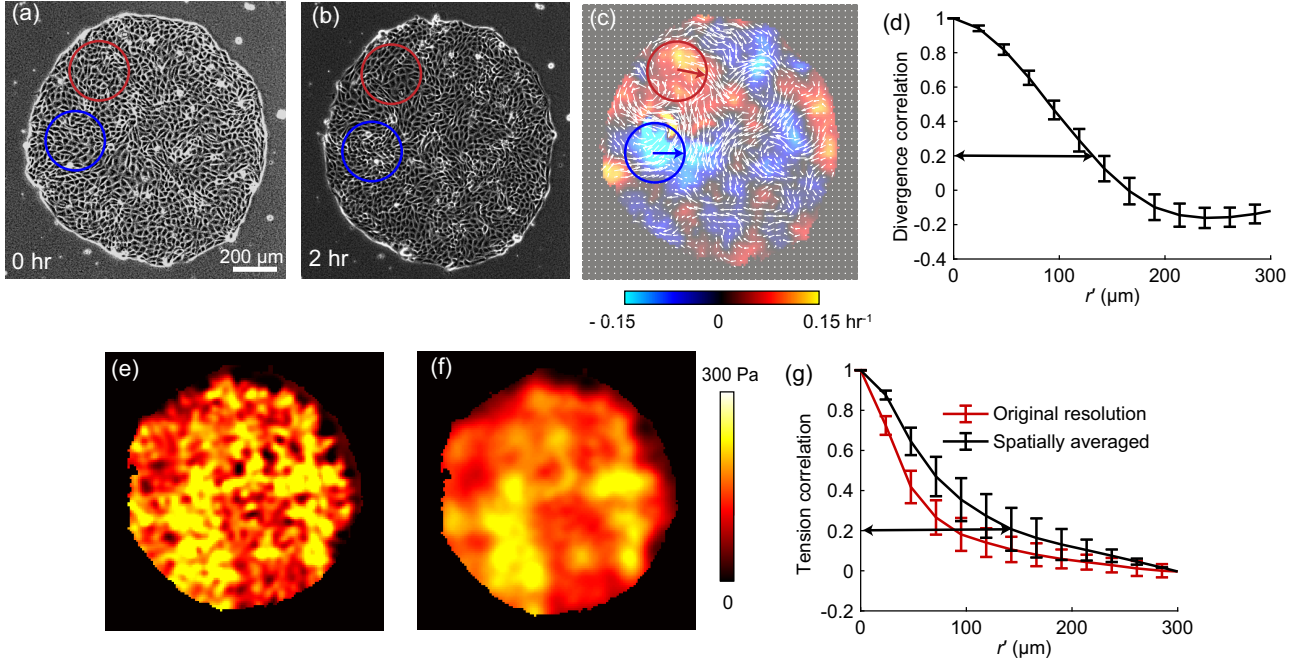


FIG. 1. Spatial correlation of $\text{div}(\vec{v})$ and contractile tension. (a, b) Phase contrast images of a cell island (diameter 1 mm) at time points separated by 2 h. The blue and red circles highlight groups of cells that decreased and increased their areas, respectively, over the 2 h. (c) Cell velocities (arrows) overlaid on a color map of $\text{div}(\vec{v})$. (d) Spatial correlation of $\text{div}(\vec{v})$ in multiple islands (diameter 1 mm). The horizontal arrow, drawn at a correlation value of 0.2, indicates the correlation length of $\text{div}(\vec{v})$. (e, f) Color map of actual (e) and spatially averaged (f) contractile tension in a cell island. (g) Spatial correlation of actual and spatially averaged contractile tension in multiple cell islands (diameter 1 mm). The horizontal arrow indicates the correlation length of spatially averaged tension. In all figures, lines with error bars indicate means and standard deviations computed over at least four cell islands.

volume. Interestingly, the cell area changes were correlated over space, meaning cells coordinated their deformations with those of their neighbors, thereby expanding and contracting in collective groups (Video 1) [37], as previously observed [9,10,36]. As an example, consider Figs. 1(a) and 1(b), showing a representative cell island at time points separated by 2 h. Between these two time points, groups of cells decreased and increased their areas; two representative groups are highlighted by the blue and red circles, respectively. To quantify the rate at which cell areas contracted and expanded, we quantified the cell velocity field, \vec{v} , with digital image correlation [26] and computed the divergence of the velocity field, $\text{div}(\vec{v})$, using Eq. (2) as in Ref. [9]. At locations where cell areas decreased or increased, the divergence was negative or positive, respectively [Figs. 1(c) and S1(b)] [37]. To verify that the measured field of divergence accurately quantified local changes in cell area, we manually tracked the areas of 20 random cells over two time points. For each of these cells, we plotted the area change against the average divergence for all data points inside the cell's periphery. The results showed a strong correlation [Fig. S1(c)] [37], implying that the measured divergence of the cell velocity field accurately quantified local changes in cell area.

Next, consistent with our visual observation of cells coordinating area changes with those of their neighbors (Video 1) [37], we observed that the sign of divergence was correlated over groups of cells. The size of a region of cells having similar divergence is an indicator of the typical size of a group of cells that collectively contracted or expanded together. To

quantify this length scale, we computed the spatial autocorrelation of $\text{div}(\vec{v})$ [Eq. (3)]. The autocorrelation decayed to zero over a distance of $\approx 200 \mu\text{m}$ [≈ 10 cell lengths, Fig. 1(d)]. We defined the correlation length of $\text{div}(\vec{v})$ to be the distance at which the autocorrelation decayed to a value of 0.2, which is the same threshold used in our prior work [34]. With this definition, the correlation length of $\text{div}(\vec{v})$ was $\approx 130 \mu\text{m}$, similar to prior observations in this cell type [9,10]. Hence, the characteristic size of a group of cells that contracted or expanded collectively was $130 \mu\text{m}$.

Since an increase in a cell's area leads to ERK-mediated contractility [11–13], we next sought to relate the area changes to the forces caused by cell contractility. As a starting point, we considered that, in a cell monolayer, changes in a cell's area are proportional to changes in that cell's contractile forces [16,38,39]. Hence, it may be that the spatial correlations in $\text{div}(\vec{v})$ are related to spatial coordination of contractile tension, which is the average normal stress transmitted between neighbors [22]. Based on this idea, we formulated a working hypothesis that the correlation length of $\text{div}(\vec{v})$ is controlled by the correlation length of contractile tension in a monolayer. To investigate the working hypothesis, we employed monolayer stress microscopy to measure the in-plane stress tensor in the cell monolayer and defined the average of the in-plane normal stresses as the contractile tension [22,30]. The contractile tension was positive, indicating that cells were in a tensile state, and it fluctuated over space, often ranging from nearly 0 to $> 300 \text{ Pa}$ [Fig. 1(e)], consistent with prior observations [22]. The fluctuations in tension occurred over

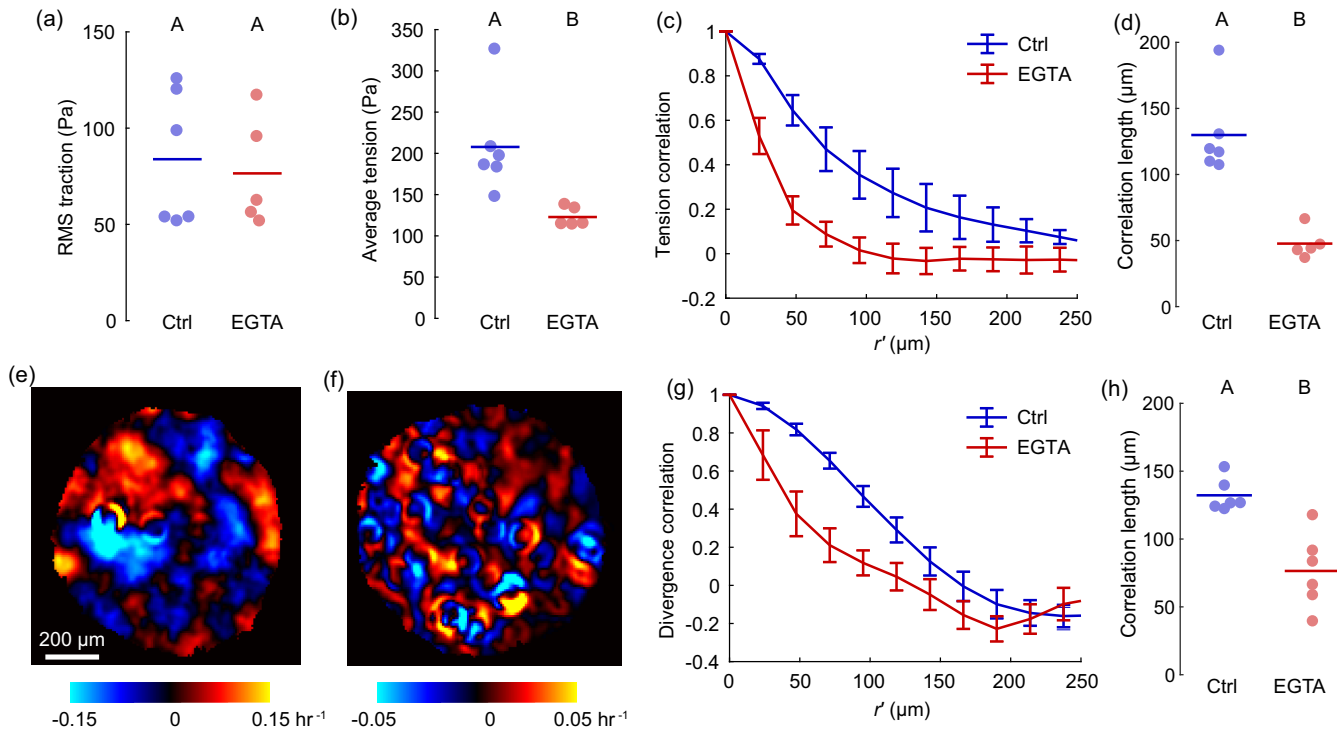


FIG. 2. Disrupting cell–cell adhesions decreased spatial correlations of contractile tension and $\text{div}(\vec{v})$. (a) RMS traction in control cell islands and islands treated with 1 mM EGTA ($p = 0.23$). (b) Average contractile tension decreased after treating with EGTA ($p = 0.012$). (c) Spatial correlation of spatially smoothed contractile tension of control and EGTA-treated islands. (d) Tension correlation length decreased after treating with EGTA ($p = 5 \times 10^{-4}$). (e, f) Color map of $\text{div}(\vec{v})$ in control (e), and EGTA-treated islands (f). (g) Spatial correlation of $\text{div}(\vec{v})$ of control and EGTA-treated islands. (h) Divergence correlation length decreased after treating with EGTA ($p = 0.0017$). Different letters (A, B) represent statistically different groups.

distances of several cell lengths, which was also consistent with prior studies [22–24]. The spatial resolution of the tension measurement ($8 \mu\text{m}$) was higher than the resolution of the measurement of $\text{div}(\vec{v})$ ($\approx 25 \mu\text{m}$), which prohibited direct comparison between the two. Therefore, the contractile tension was spatially smoothed to attain a spatial resolution matching that of $\text{div}(\vec{v})$ [Methods, Fig. 1(f)]. As expected, the spatial autocorrelation of tension indicated that the smoothing increased the correlation slightly [Fig. 1(g)]. The distance over which the autocorrelation of smoothed tension decreased to a value of 0.2 was defined as the correlation length, and it was $\approx 140 \mu\text{m}$ [Fig. 1(g)]. Hence, the correlation length of tension was similar in magnitude to that of $\text{div}(\vec{v})$ ($140 \mu\text{m}$ compared $130 \mu\text{m}$), which was consistent with our working hypothesis and motivated further investigation of the relationship between the two.

As a first test of our working hypothesis, we attempted to alter the correlation length of $\text{div}(\vec{v})$ by perturbing the correlation length of tension. The most obvious way to perturb the tension correlation length was via the cell–cell adhesions that transmit contractile tension through the cell layer. Indeed, a prior study quantified tensile stress in response to perturbing cell–cell adhesions in various different ways, including knockout of the adherens junction proteins E- and P-cadherin and by knockout of α - and β -catenin, which connect adherens junctions to the cytoskeleton. In response to these knockouts, the maps of tensile stress appeared qualitatively to fluctuate more quickly over space, suggesting reduced tension correlation

length [40]. Similarly, other studies showed that disruption of adherens junctions by chelating calcium or knockout of α -catenin altered the collective motion by suppressing plithotaxis, the tendency of cells to migrate along directions of maximal principal stress [22], and by suppressing collective durotaxis, the tendency for a cell collective to migrate towards regions of greater substrate stiffness [41]. Leveraging these prior findings, we designed an experiment to reduce the tension correlation length by disrupting the cell–cell adhesions, enabling us to test our working hypothesis that the correlation length of $\text{div}(\vec{v})$ is controlled by the correlation length of contractile tension. Similar to prior studies [22,42–44], we used a chelator for calcium, which is necessary for cadherin-based adherens junctions. We chose ethylene glycol tetraacetic acid (EGTA), and because calcium is necessary for cell contractility, we used a low concentration (1 mM), in an effort to perturb adhesions but not contractility in islands of 1 mm diameter. Since cell number density can affect cell contractility in a monolayer [16,39,45,46], we verified that our seeding of the cells into islands kept the density (equivalently, the inverse of average cell area) nearly constant [Fig. S2(a)] [37]. To verify contractility was unaltered from EGTA treatment, we first quantified the field of cell–substrate traction. The root-mean-square (RMS) of traction of control and calcium-chelated cells were no different, suggesting that the chelation did not have a significant effect on the cell contractility [Fig. 2(a)]. However, the mean contractile tension decreased by approximately 40% [Figs. 2(b), S2(b), and S2(c)] [37], indicating reduced stresses

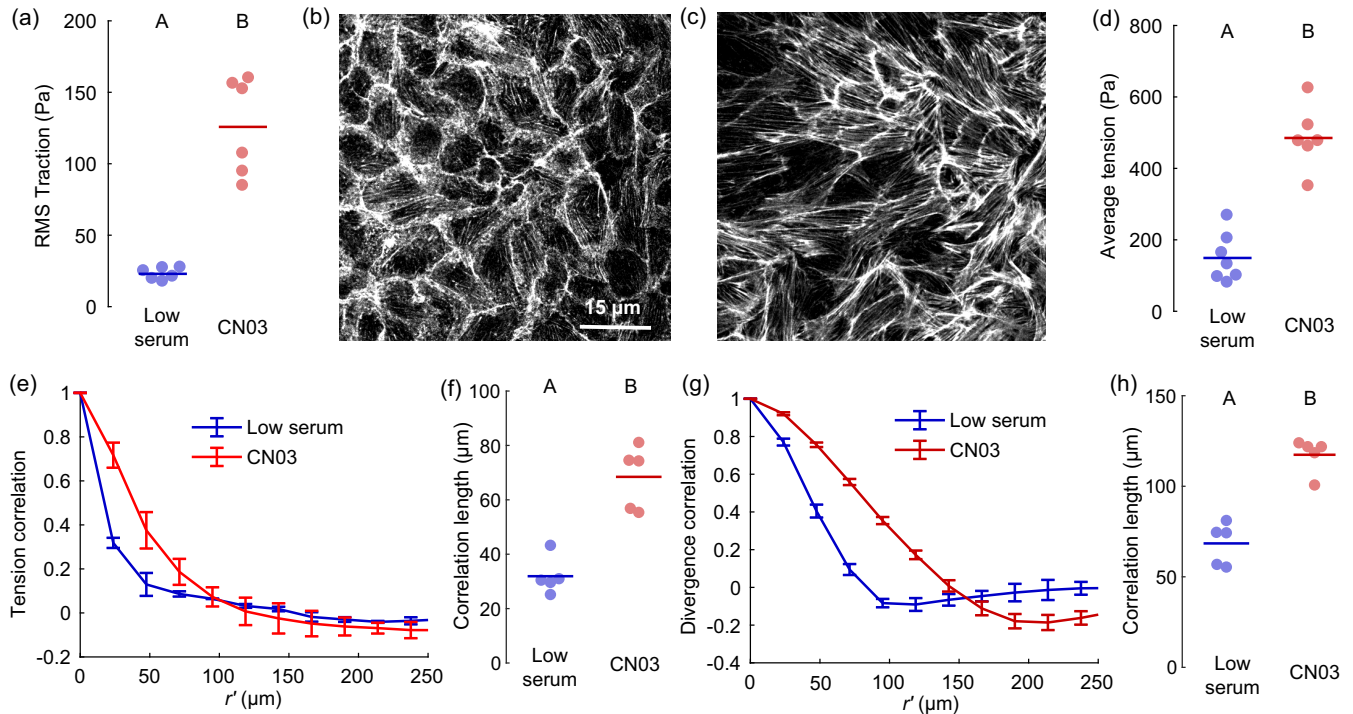


FIG. 3. Rho activator CN03 increased the spatial correlation of contractile tension and $\text{div}(\vec{v})$. (a) The RMS traction was increased by a factor of 5 after treating with $4 \mu\text{g/ml}$ CN03 ($p = 0.3 \times 10^{-4}$). (b, c) Confocal images of stress fibers of low serum (b) and CN03-treated conditions (c). (d) Average contractile tension was increased by a factor of 2.5 after treating with CN03 ($p = 0.3 \times 10^{-4}$). (e) Spatial correlation of contractile tension in low serum and CN03-treated conditions. (f) The spatial correlation of contractile tension was increased in response to treatment with CN03 compared to low serum conditions ($p = 0.4 \times 10^{-5}$). (g) Spatial correlation of divergence in low serum and CN03-treated conditions. (h) The spatial correlation of $\text{div}(\vec{v})$ was increased in response to treatment with CN03 compared to low serum conditions ($p = 0.4 \times 10^{-4}$). Different letters (A, B) represent statistically different groups.

at the cell-cell interface, consistent with reduced cell-cell adhesions and consistent with prior findings [22]. As expected, the EGTA treatment decreased the tension correlation length by approximately 60% from 125 to $50 \mu\text{m}$ [Figs. 2(c) and 2(d)]. Additionally, the treatment decreased the correlation length of $\text{div}(\vec{v})$ by approximately 40% from 130 to $75 \mu\text{m}$ [Figs. 2(e)–2(h); Videos 1 and 2] [37], consistent with our working hypothesis that the correlation length of $\text{div}(\vec{v})$ results from the correlation length of tension.

To design a second test of our working hypothesis, we sought to identify another factor that would affect the correlation length of contractile tension. To this end, we considered our recent observation that neighboring cells coordinate so as to align the direction of traction applied to the substrate [34]. We showed that coordination of traction was affected by the Rho activator CN03, which caused greater alignment of both stress fibers and tractions between neighboring cells as compared to cells in low serum conditions [34]. As force equilibrium dictates that cell-substrate tractions balance with contractile tension [22,30], we reasoned that traction alignment could increase the correlation length of tension, thereby increasing the correlation length of $\text{div}(\vec{v})$. To test this reasoning, we seeded 1 mm diameter islands, verified the cell density was approximately constant [Fig. S3(a)] [37], and treated with CN03 or a vehicle control. Consistent with our previous observations, activating CN03 increased the RMS traction [Fig. 3(a)] and increased the alignment of stress fibers between neighboring cells [Figs. 3(b) and 3(c)]. To balance

the increased traction, the average contractile tension also increased [Fig. 3(d)]. Consistent with our expectation, the average spatial correlation length of the contractile tension was larger ($70 \mu\text{m}$) in CN03-treated cells compared to control ($30 \mu\text{m}$) [Figs. 3(e) and 3(f)] as was the average correlation length of $\text{div}(\vec{v})$ [$120 \mu\text{m}$ compared to $69 \mu\text{m}$, Figs. 3(g) and 3(h); Videos 3 and 4] [37]. Hence, to balance the increased coordination of cell-substrate traction between neighboring cells, cells exhibited increased spatial coordination of contractile tension, which in turn increased the correlation length of $\text{div}(\vec{v})$, again supporting our working hypothesis that the correlation length of tension affects the correlation length of $\text{div}(\vec{v})$.

We next designed an experiment to perturb the spatial correlation of contractile tension using methods other than chemical treatments. Considering that the finite size of a cell island may limit the distance over which contractile tension propagates through cell-cell adhesions, we expected that increasing and decreasing the diameter of the islands on which the cells were seeded would respectively increase and decrease the correlation length of tension. We repeated the experiments in islands of diameters 0.5, 1.5, and 3 mm (Videos 5–7) [37], while keeping the cell seeding density approximately constant [Fig. S3(b)] [37]. As expected, the spatial correlation of contractile tension depended on island size. For smaller islands (diameter 0.5 mm), the tension correlation length was reduced, and for larger islands (1.5 and 3 mm) it was increased [Figs. 4(a) and 4(b)]. The overall range

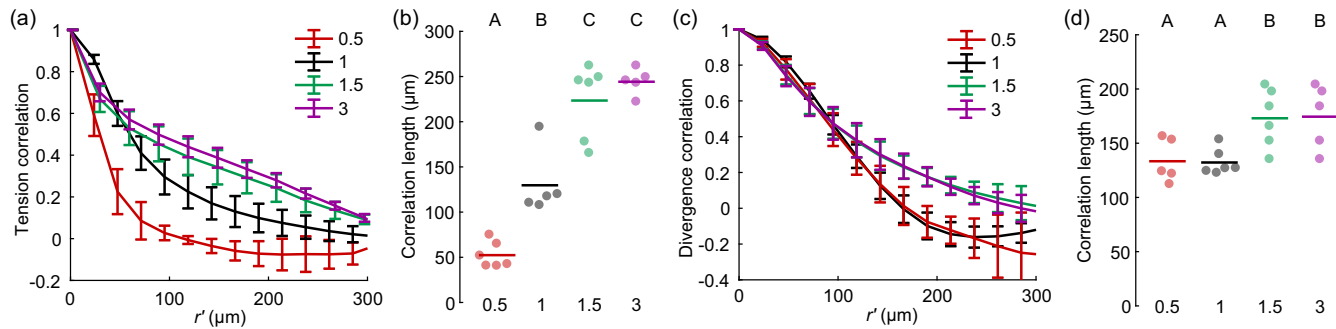


FIG. 4. Effect of island size on contractile tension and divergence in a cell monolayer. (a) Spatial correlation of contractile tension in islands of diameter 0.5, 1, 1.5, and 3 mm. (b) Correlation length of tension for islands of different diameter ($p = 0.0012$, 4×10^{-7} , and 4×10^{-9} for diameters of 1, 1.5, and 3 mm compared to 0.5 mm). (c) Spatial correlation of $\text{div}(\vec{v})$ in islands of diameter 0.5, 1, 1.5, and 3 mm. (d) Correlation length of $\text{div}(\vec{v})$ for islands of different diameter ($p = 0.91$, 0.012, and 0.033 for diameters of 1, 1.5, and 3 mm compared to 0.5 mm). Different letters (A, B, C) represent statistically different groups.

of tension correlation length was from $50 \mu\text{m}$ (for the smallest islands) to $240 \mu\text{m}$ (largest islands). Additionally, for the two largest islands, the correlation lengths were not statistically different, suggesting saturation at a correlation length of $\approx 240 \mu\text{m}$ for islands of diameter ≥ 1.5 mm. This correlation length was slightly larger than the correlation length in a prior study in large (>3 mm) cell monolayers [22], which is reasonable given that the smoothing of tension that we performed increased the correlation length [Figs. 1(e)–1(g)]. Next, we computed the spatial correlation of $\text{div}(\vec{v})$. The correlation length of $\text{div}(\vec{v})$ was larger ($\approx 175 \mu\text{m}$) for islands of diameters 1.5 and 3 mm compared to 0.5 and 1 mm ($\approx 130 \mu\text{m}$) [Figs. 4(c) and 4(d)], which is similar to the trends in the correlation length of tension [Figs. 4(a) and 4(b)]. The correlation length of $\text{div}(\vec{v})$ was not statistically different for islands of 0.5 and 1 mm diameter, which did not match the trends observed for tension correlation length and may be explained by the fact that the magnitude of $\text{div}(\vec{v})$ differed for these island sizes (Fig. S4; see the Supplemental Material for more details on the effects of island size on $\text{div}(\vec{v})$ [37]). We also note that that magnitudes of both tension and cell speed decreased with increasing island size (Figs. S4(d) and S4(e) [37]), consistent with a prior study [47]. In summary, the trend from these data was that, in response to increasing island size, the correlation lengths of $\text{div}(\vec{v})$ and tension increased together, in agreement with our working hypothesis that the correlation length of tension affects the correlation length of $\text{div}(\vec{v})$.

With evidence that tension in the cell monolayer is responsible for correlations over space, the remaining question is how spatial correlations in tension combine with mechanisms of signal transduction inside each cell to produce spatial correlations in $\text{div}(\vec{v})$. To answer this question, we considered that tension and $\text{div}(\vec{v})$ are related through mechanochemical signaling by the ERK pathway [11,12,14,15]. Prior studies considering effects of ERK activation on cell motion presented images in which activated ERK appeared to be spatially correlated over ≈ 6 – 8 cell lengths [12,13,17,18]. Since activated ERK is thought to trigger cell contraction, and given that there exist spatial correlations in both ERK and contractile tension, it is reasonable to hypothesize that there is a relationship between ERK activation and contractile tension. To

investigate this proposed relationship, we reduced ERK activity by inhibiting the ERK kinases MEK1 and MEK2 using different concentrations of U0126 (10 and $40 \mu\text{M}$), while keeping the cell density approximately constant [Fig. S3(c)] [37]. Consistent with the understanding that ERK activates cell contractility [11,12,14,15], the mean contractile tension decreased in response to the higher concentration of U0126 [Fig. 5(a)]. Surprisingly, neither concentration of the inhibitor affected the correlation length of contractile tension which remained approximately at $100 \mu\text{m}$ [Figs. 5(b) and 5(c)]. Similarly, in islands of different size (both 0.5 and 1.5 mm), the tension correlation length was unaffected by either concentration of the inhibitor [Fig. S5(a)] [37], suggesting that ERK was not the underlying cause of spatial correlations in tension. Additionally, immunofluorescent staining for phosphorylated ERK (pERK) showed that the spatial correlation length of ERK activation was unaffected [Figs. S6(a)–S6(d)] [37], which is reminiscent of the unchanged correlation length of tension [Figs. 5(b) and 5(c)]. These findings can be combined with Figs. 2–4, which demonstrated how different methods to perturb equilibrium of forces within the cell layer changed the correlation length of tension, to suggest that the correlation length of tension results primarily from the physical equilibrium of force across the cell layer.

Despite the fact that inhibiting ERK activity had no effect on the tension correlation length [Figs. 5(b) and 5(c)], it caused a dose-dependent decrease in the correlation length of $\text{div}(\vec{v})$ from $130 \mu\text{m}$ to as small as $58 \mu\text{m}$ in 1 mm islands [Figs. 5(d) and 5(e); Videos 8–10] [37]. Similar trends were observed in 0.5 and 1.5 mm islands as well [Fig. S5(b)] [37]. Furthermore, the RMS of $\text{div}(\vec{v})$ was also decreased [Fig. S6(e)] [37]. The effect of the inhibitor on the divergence correlation length suggests that ERK-mediated cell contractility is somehow related to the spatial correlation of $\text{div}(\vec{v})$. To understand the effect of ERK activity on the correlation length of $\text{div}(\vec{v})$, it is necessary to first describe the current understanding of how ERK couples changes in cell area with cell contractility. After a cell's area is increased, ERK is activated, which causes an increase in cell contractility [11–13]. In turn, the increased contractility is thought to reduce the cell's area [13]. This understanding suggests that there would be a proportional relationship between cell area and tension

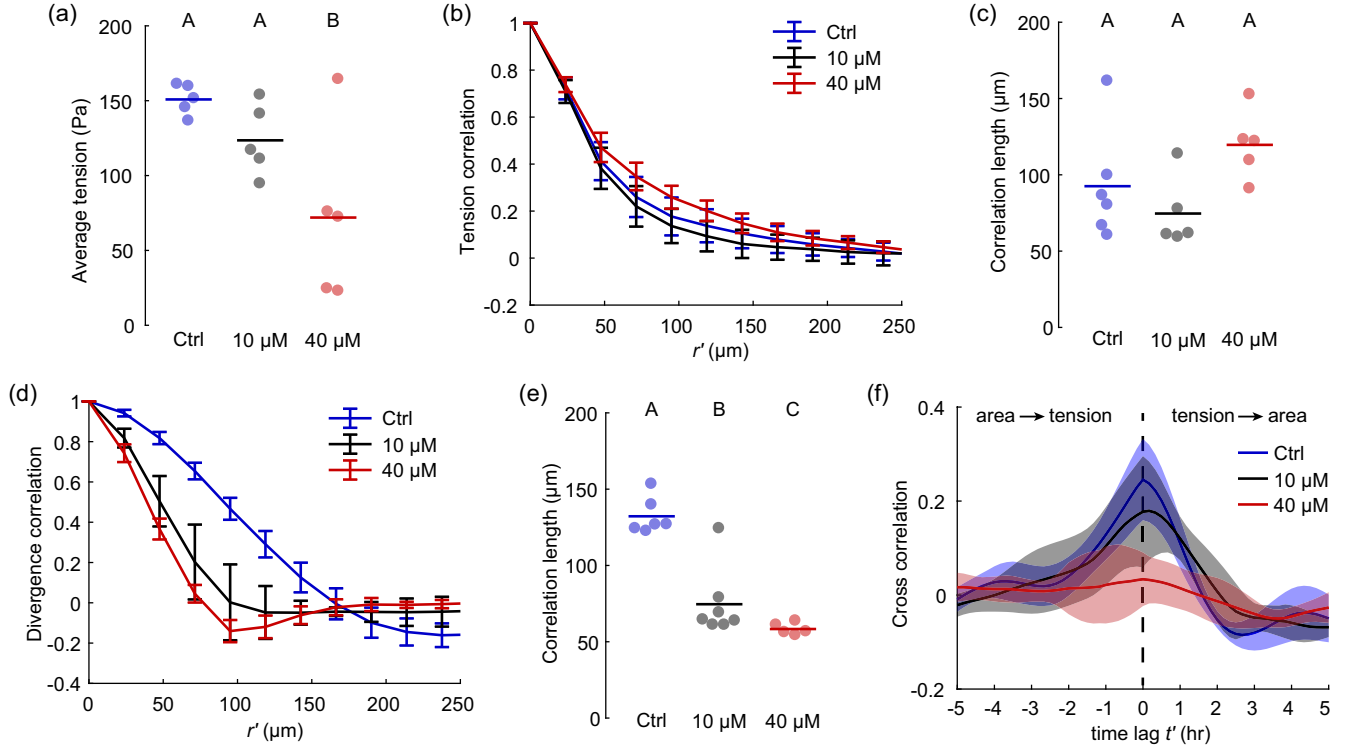


FIG. 5. Inhibiting ERK decreased spatial correlation of $\text{div}(\vec{v})$ by disrupting interplay between cell area and tension. (a) Average tension in response to treating cell islands (diameter 1 mm) with U0126. While 10 μM had no significant effect on average tension ($p = 0.31$ compared to control), 40 μM decreased the average tension ($p = 0.0053$ compared to control). (b) Spatial correlation of contractile tension in control islands and islands treated with U0126. (c) Tension correlation length remained unchanged in response to 10 μM ($p = 0.32$ compared to control) and 40 μM ($p = 0.46$ compared to control) U0126. (d) Spatial correlation of $\text{div}(\vec{v})$ in control islands and islands treated with U0126. (e) Correlation length of $\text{div}(\vec{v})$ decreased in response to 10 μM ($p = 0.0051$ compared to control) and 40 μM ($p = 0.0017$ compared to control) U0126. (f) Temporal cross-correlation of contractile tension and cell area for control islands and islands treated with U0126. The peak of the cross-correlation decreased with increased concentration of U0126. Lines and shading represent means and standard deviations over at least four cell islands. Different letters (A, B, C) represent statistically different groups.

[16,38,39]. To test for such a relationship, we first measured cell areas using Voronoi-based cell outlines (Methods), as previously performed [8,13,34]. We also verified that error in the Voronoi-based measurement of cell area was small by comparing to manually-tracked cell areas [Figs. S7(a) and S7(b)] [37]. Next, we measured the contractile tension, mapped it to each Voronoi-based cell outline, and computed the average tension in each cell (Methods). The error in the measurements of Voronoi-based contractile tension was again small [Figs. S7(c) and S7(d)] [37]. Using these single cell data of area and tension, we computed a temporal cross-correlation between cell area and tension [Eq. (4)]. In control conditions, the peak of the cross-correlation occurred at a time lag of $t' = 0$ [Fig. 5(f)], indicating that when a cell's area increased, the corresponding increase in tension was faster than our temporal resolution of 10 min. Interestingly, the cross correlation exhibited anticorrelation at a time lag of 170 min [Fig. 5(f)], indicating that when a cell's tension increased, contraction in cell area required an additional 170 min. Moreover, the anticorrelation occurred only for positive time lags, implying that changes in the contractile tension precede—rather than follow—changes in the cell area, suggesting that increased cell contractility decreased the cell area. The positive and negative peaks were robust, as they were also present in islands of different size (Fig. S8) [37]. In response to

low and high concentrations of U0126, the positive peak of the cross-correlation decreased and disappeared, respectively [Fig. 5(f)], indicating that inhibiting ERK activation disrupted the mechanism whereby increases in cell area caused increases in contractile tension. This finding explains how the correlation length of $\text{div}(\vec{v})$ was affected by U0126 even when the correlation length of tension was not: even though tension remained correlated over space, the inhibitor disrupted the relationship between area and tension within each cell, thereby blocking the biophysical mechanism whereby spatial correlations in tension led to spatial correlations in $\text{div}(\vec{v})$.

IV. DISCUSSION

Prior studies have shown that in a monolayer, cell areas increase and decrease over time [9,10,36], and that such area changes can activate ERK, in turn leading to increased cell contraction [11,12,14,15]. Still unclear is the underlying cause of the observation that cells expand and contract in collective groups, causing area changes to be correlated over space. Here, we studied the factors underlying such spatial correlation, with our working hypothesis being that the transfer of forces across the cell layer sets a length scale for collective cell contraction and expansion. To test our hypothesis, we perturbed the spatial correlation of contractile tension by

disrupting cell-cell adhesions, increasing alignment of tractions between neighboring cells, and changing the size of the cell monolayer. In all cases, the spatial correlation lengths of tension and $\text{div}(\bar{v})$ increased or decreased together, consistent with our hypothesis. To relate these findings to the intracellular mechanisms relating force and area, we inhibited ERK activation, which reduced the correlation length of $\text{div}(\bar{v})$ but not tension. Hence, coordinated expansion and contraction between neighboring cells requires ERK signaling, to connect area and force within each cell, and force equilibrium, to transmit forces over space.

In this study, we defined the tension as half the trace of the stress tensor within the plane of the cell monolayer, computed by applying the principle of force equilibrium to the field of cell-substrate tractions [22,30]. Our definition of tension differs from the concept of a line tension, which has units of force per distance, occurs at the cell edges, and is analogous to surface tension of a fluid. Line tension is frequently referred to as “tension” in studies using vertex models [21,48–52], and methods have been proposed to measure it by applying the principle of force equilibrium to segmented images of a cell layer [53–56]. The line tension is important in systems wherein tractions (and hence components of the in-plane stress tensor) are small, such as the developing embryo. For example, models have suggested that in such systems, line tension sets a preferred perimeter that controls a rigidity transition [49,50], and line tension supports the majority of the forces required by intercellular equilibrium, enabling cells to change their areas with minimal energy cost [52]. By contrast, the cells in our experiments adhered and applied tractions to the substrate. In such a system, the effects of the tractions and the associated force balance can dominate over those of line tension. For example, experiments in monolayers of adherent cells have shown that cell shape and motion are controlled more so by tractions than line tension [25], which is consistent with modeling showing that a rigidity transition can also be caused by cell traction forces [51]. Therefore, in this work, we focused on the tension measured by applying the principle of equilibrium to the cell-substrate tractions, which is likely to have the largest effects on cell motion and area changes.

The ERK pathway is central to waves of cell contraction and motion that propagate across the cell layer, as shown in many prior studies [12–17]. A central component of the role of ERK is that ERK activation is thought to lead to an increase in contractile tension, which in turn causes a reduction in cell area [12,13,17]. Aspects of the connection between ERK, tension, and area have been measured, for example, by relating ERK activation to changes in area through a cross-correlation [12,13], but still lacking was a measurement of tension. Here, we explicitly measured both tension and area within the cell layer, enabling us to relate them by a temporal cross-correlation. The positive peak at zero time lag indicates that the time delay between changes in area and tension was less than our temporal resolution of 10 min. Prior measurements [12,13] showed that the time between cell stretching and ERK activation is 3–4 min. This finding, when combined with our data and the understanding that cell stretching causes ERK activation, which in turn causes increased tension, would suggest that the time delay between ERK activation and increased tension is no longer than a

few minutes. Following increased tension, an anticorrelation between tension and area occurred at a time lag of 170 min, which is a new measurement demonstrating that a decrease in cell area followed from increased cell contractility. The 170 min is similar in magnitude to a recently observed time lag of 2–3 h between ERK activation and decreases of cell area [13]. The magnitude of the time lag between tension and cell contraction (170 min) was far larger than the lag between cell stretching and tension (<10 min), which suggests the existence of some viscoelastic mechanism responsible for the time delay. One potential mechanism may be the flow of fluid through intercellular junctions, which, in monolayers of this cell type, occurs on the same timescale [9].

The correlation between tension and area at short time lag [Fig. 5(f)] indicates a monotonic relationship between the two, which is reminiscent of elastic behavior. An apparent elastic behavior has been observed in prior studies of cell monolayers as well, with efforts to quantify it in terms of an effective elastic modulus [16,39,57]. Importantly, in this study, the apparent elasticity results not from mechanical properties alone, but also from ERK signaling, as demonstrated by our findings that the correlation between tension and area depends on ERK activity. Consistent with this finding is the prior observation that at higher cell density (equivalently, smaller average cell area), ERK activity is reduced [58]. Hence, the apparent elastic behavior is an active phenomenon, mediated by the ERK pathway. It is common for theoretical models for cell collectives to use equations that produce an elastic relationship, modeling the cells as an elastic continuum [16,59], as particles having elastic interactions between neighbors [60,61], or as sets of vertices outlining polygons having a preferred area [49–51]. Our finding that ERK signaling mediates the relationship between cell tension and area gives an explanation for the underlying cause of the apparent elastic behavior, and justifies the use of elastic behavior in the theoretical models. It should be noted that the rheology of the cell layer is not fully elastic, however, because over long timescales, cells can rearrange positions with their neighbors with no memory of their prior positions. Such flow can be achieved in the particle and vertex models, wherein the elastic behavior is imposed on each cell but not on the entire cell layer. An elastic behavior may be important to maintain integrity of the epithelium, as the proportional relationship between cell size and tension would mean that more force is required to stretch a large cell as compared to a small cell, which would prevent excessive deformation. This idea has been observed *in vivo* in the developing *Drosophila* dorsal thorax, wherein cells with larger area exhibit more apical stress fibers and hence greater tension [62]. Interestingly, elevated tension also stimulates Hippo signaling, leading to increased proliferation rates in cells having larger area [62], which could be a second mechanism whereby the apparent elastic relationship between cell area and tension acts to maintain tissue integrity.

Whereas the elastic behavior appears to be at the level of the single cell, force equilibrium dictates that tensile forces are balanced between neighboring cells, hence producing a spatial correlation of tension [22]. The tension correlation is unlikely to result solely from passive force equilibrium, because in epithelial cells, phosphorylated myosin light chain appears to be correlated in space, with clusters of cells exhibiting

similar levels of phosphorylated myosin light chain, implying similar magnitudes of active contraction in neighboring cells [20,21]. Additionally, neighboring cells can coordinate their cytoskeletal organization to create multicellular actomyosin cables [63]. Through this coordination, the cells gain control over which direction the tension is produced and transmitted, which can be useful, for example, in facilitating cell rearrangements that are required for narrowing and elongation of tissues during development [64]. The multicellular actomyosin cables also make tissue shape changes robust to both damage of a cable and to noise caused by local fluctuations in myosin contraction [65,66]. An underlying theme in these examples and in our study is that coordination of cell contraction means that neighboring cells cooperate rather than compete [67], which enables deformations to occur on length

scales larger than a single cell. Hence, the transmission of force across an epithelial cell layer is essential for controlling tissue size and shape.

ACKNOWLEDGMENTS

We thank Dr. Brian Burkel and members of the Notbohm laboratory for helpful discussions. Confocal microscopy was performed at the University of Wisconsin-Madison Biochemistry Optical Core and in Christian Franck's laboratory with assistance from Harry C. Cramer III. This work was supported by the University of Wisconsin-Madison Office of the Vice Chancellor for Research and Graduate Education with funding from the Wisconsin Alumni Research Foundation and National Science Foundation Grant No. CMMI-1660703.

-
- [1] M. Leptin, Gastrulation movements: The logic and the nuts and bolts, *Dev. Cell* **8**, 305 (2005).
- [2] T. Lecuit and P.-F. Lenne, Cell surface mechanics and the control of cell shape, tissue patterns and morphogenesis, *Nat. Rev. Mol. Cell Biol.* **8**, 633 (2007).
- [3] P.-A. Pouille, P. Ahmadi, A.-C. Brunet, and E. Farge, Mechanical signals trigger myosin II redistribution and mesoderm invagination in drosophila embryos, *Sci. Signal.* **2**, ra16 (2009).
- [4] T. Zulueta-Coarasa and R. Fernandez-Gonzalez, Dynamic force patterns promote collective cell movements during embryonic wound repair, *Nat. Phys.* **14**, 750 (2018).
- [5] R. J. Tetley, M. F. Staddon, D. Heller, A. Hoppe, S. Banerjee, and Y. Mao, Tissue fluidity promotes epithelial wound healing, *Nat. Phys.* **15**, 1195 (2019).
- [6] L. E. Wickert, S. Pomeranke, I. Mitchell, K. S. Masters, and P. K. Kreeger, Hierarchy of cellular decisions in collective behavior: Implications for wound healing, *Sci. Rep.* **6**, 20139 (2016).
- [7] E. Gauquelin, S. Tlili, C. Gay, G. Peyret, R.-M. Mège, M. A. Fardin, and B. Ladoux, Influence of proliferation on the motions of epithelial monolayers invading adherent strips, *Soft Matter* **15**, 2798 (2019).
- [8] S. M. Zehnder, M. Suaris, M. M. Bellaire, and T. E. Angelini, Cell volume fluctuations in MDCK monolayers, *Biophys. J.* **108**, 247 (2015).
- [9] S. M. Zehnder, M. K. Wiatt, J. M. Uruena, A. C. Dunn, W. G. Sawyer, and T. E. Angelini, Multicellular density fluctuations in epithelial monolayers, *Phys. Rev. E* **92**, 032729 (2015).
- [10] R. Thiagarajan, A. Bhat, G. Salbreux, M. M. Inamdar, and D. Rivelino, Pulsations and flows in tissues: two collective dynamics with simple cellular rules, *bioRxiv* (2020), doi: 10.1101/2020.07.29.226357.
- [11] H.-J. Hsu, C.-F. Lee, A. Locke, S. Q. Vanderzyl, and R. Kaunas, Stretch-induced stress fiber remodeling and the activations of JNK and ERK depend on mechanical strain rate, but not FAK, *PLoS One* **5**, e12470 (2010).
- [12] N. Hino, L. Rossetti, A. Marín-Llauradó, K. Aoki, X. Trepát, M. Matsuda, and T. Hirashima, ERK-mediated mechanochemical waves direct collective cell polarization, *Dev. Cell* **53**, 646 (2020).
- [13] D. Boockock, N. Hino, N. Ruzickova, T. Hirashima, and E. Hannezo, Theory of mechanochemical patterning and optimal migration in cell monolayers, *Nat. Phys.* **17**, 267 (2021).
- [14] Y. Matsubayashi, M. Ebisuya, S. Honjoh, and E. Nishida, ERK activation propagates in epithelial cell sheets and regulates their migration during wound healing, *Curr. Biol.* **14**, 731 (2004).
- [15] D. L. Nikolic, A. N. Boettiger, D. Bar-Sagi, J. D. Carbeck, and S. Y. Shvartsman, Role of boundary conditions in an experimental model of epithelial wound healing, *Am. J. Physiol. Cell Physiol.* **291**, C68 (2006).
- [16] J. Notbohm, S. Banerjee, K. J. Utuje, B. Gweon, H. Jang, Y. Park, J. Shin, J. P. Butler, J. J. Fredberg, and M. C. Marchetti, Cellular contraction and polarization drive collective cellular motion, *Biophys. J.* **110**, 2729 (2016).
- [17] K. Aoki, Y. Kondo, H. Naoki, T. Hiratsuka, R. E. Itoh, and M. Matsuda, Propagating wave of ERK activation orients collective cell migration, *Dev. Cell* **43**, 305 (2017).
- [18] Y. Ogura, F.-L. Wen, M. M. Sami, T. Shibata, and S. Hayashi, A switch-like activation relay of EGFR-ERK signaling regulates a wave of cellular contractility for epithelial invagination, *Dev. Cell* **46**, 162 (2018).
- [19] A. D. Simone, M. N. Evanitsky, L. Hayden, B. D. Cox, J. Wang, V. A. Tornini, J. Ou, A. Chao, K. D. Poss, and S. D. Talia, Control of osteoblast regeneration by a train of ERK activity waves, *Nature (London)* **590**, 129 (2021).
- [20] A. J. Loza, S. Koride, G. V. Schimizzi, B. Li, S. X. Sun, and G. D. Longmore, Cell density and actomyosin contractility control the organization of migrating collectives within an epithelium, *Mol. Biol. Cell* **27**, 3459 (2016).
- [21] S. Koride, A. J. Loza, and S. X. Sun, Epithelial vertex models with active biochemical regulation of contractility can explain organized collective cell motility, *APL Bioeng.* **2**, 031906 (2018).
- [22] D. T. Tambe, C. C. Hardin, T. E. Angelini, K. Rajendran, C. Y. Park, X. Serra-Picamal, E. H. Zhou, M. H. Zaman, J. P. Butler, D. A. Weitz, J. J. Fredberg, and X. Trepát, Collective cell guidance by cooperative intercellular forces, *Nat. Mater.* **10**, 469 (2011).
- [23] T. Das, K. Safferling, S. Rausch, N. Grabe, H. Boehm, and J. P. Spatz, A molecular mechanotransduction pathway regulates collective migration of epithelial cells, *Nat. Cell Biol.* **17**, 276 (2015).
- [24] M. Vishwakarma, J. D. Russo, D. Probst, U. S. Schwarz, T. Das, and J. P. Spatz, Mechanical interactions among followers determine the emergence of leaders in migrating epithelial cell collectives, *Nat. Commun.* **9**, 3469 (2018).

- [25] A. Saraswathibhatla and J. Notbohm, Traction and Stress Fibers Control Cell Shape and Rearrangements in Collective Cell Migration, *Phys. Rev. X* **10**, 011016 (2020).
- [26] E. Bar-Kochba, J. Toyjanova, E. Andrews, K.-S. Kim, and C. Franck, A fast iterative digital volume correlation algorithm for large deformations, *Exp. Mech.* **55**, 261 (2014).
- [27] J. P. Butler, I. M. Tolić-Nørrelykke, B. Fabry, and J. J. Fredberg, Traction fields, moments, and strain energy that cells exert on their surroundings, *Am. J. Physiol. Cell Physiol.* **282**, C595 (2002).
- [28] J. C. del Alamo, R. Meili, B. Alonso-Latorre, J. Rodriguez-Rodriguez, A. Aliseda, R. A. Firtel, and J. C. Lasheras, Spatio-temporal analysis of eukaryotic cell motility by improved force cytometry, *Proc. Natl. Acad. Sci. USA* **104**, 13343 (2007).
- [29] X. Trepát, M. R. Wasserman, T. E. Angelini, E. Millet, D. A. Weitz, J. P. Butler, and J. J. Fredberg, Physical forces during collective cell migration, *Nat. Phys.* **5**, 426 (2009).
- [30] D. T. Tambe, U. Croutelle, X. Trepát, C. Y. Park, J. H. Kim, E. Millet, J. P. Butler, and J. J. Fredberg, Monolayer stress microscopy: Limitations, artifacts, and accuracy of recovered intercellular stresses, *PLoS One* **8**, e55172 (2013).
- [31] <https://github.com/jknotbohm/Cell-Traction-Stress>.
- [32] A. Saraswathibhatla, E. E. Galles, and J. Notbohm, Spatiotemporal force and motion in collective cell migration, *Sci. Data* **7**, 197 (2020).
- [33] U. Schmidt, M. Weigert, C. Broaddus, and G. Myers, Cell detection with star-convex polygons, in *Medical Image Computing and Computer Assisted Intervention (MICCAI'18)* (Springer International Publishing, Berlin, 2018), pp. 265–273.
- [34] A. Saraswathibhatla, S. Henkes, E. E. Galles, R. Sknepnek, and J. Notbohm, Coordinated tractions increase the size of a collectively moving pack in a cell monolayer, *Extreme Mech. Lett.* **48**, 101438 (2021).
- [35] S. Kaliman, C. Jayachandran, F. Rehfeldt, and A.-S. Smith, Limits of applicability of the Voronoi tessellation determined by centers of cell nuclei to epithelium morphology, *Front. Physiol.* **7**, 551 (2016).
- [36] C. Blanch-Mercader, V. Yashunsky, S. Garcia, G. Duclos, L. Giomi, and P. Silberzan, Turbulent Dynamics of Epithelial Cell Cultures, *Phys. Rev. Lett.* **120**, 208101 (2018).
- [37] See Supplemental Material at <http://link.aps.org/supplemental/10.1103/PhysRevE.105.024404> for additional figures and videos.
- [38] X. Serra-Picamal, V. Conte, R. Vincent, E. Anon, D. T. Tambe, E. Bazellieres, J. P. Butler, J. J. Fredberg, and X. Trepát, Mechanical waves during tissue expansion, *Nat. Phys.* **8**, 628 (2012).
- [39] R. Vincent, E. Bazellieres, C. Pérez-González, M. Uroz, X. Serra-Picamal, and X. Trepát, Active Tensile Modulus of an Epithelial Monolayer, *Phys. Rev. Lett.* **115**, 248103 (2015).
- [40] E. Bazellieres, V. Conte, A. Elosegui-Artola, X. Serra-Picamal, M. Bintanel-Morcillo, P. Roca-Cusachs, J. J. Muñoz, M. Sales-Pardo, R. Guimerà, and X. Trepát, Control of cell-cell forces and collective cell dynamics by the intercellular adhesive, *Nat. Cell Biol.* **17**, 409 (2015).
- [41] R. Sunyer, V. Conte, J. Escribano, A. Elosegui-Artola, A. Labernadie, L. Valon, D. Navajas, J. M. Garcia-Aznar, J. J. Muñoz, P. Roca-Cusachs, and X. Trepát, Collective cell durotaxis emerges from long-range intercellular force transmission, *Science* **353**, 1157 (2016).
- [42] A. Cziráok, K. Varga, E. Méhes, and A. Szabó, Collective cell streams in epithelial monolayers depend on cell adhesion, *New J. Phys.* **15**, 075006 (2013).
- [43] K. E. Worley, D. Shieh, and L. Q. Wan, Inhibition of cell-cell adhesion impairs directional epithelial migration on micropatterned surfaces, *Integr. Bio.* **7**, 580 (2015).
- [44] G. Shim, D. Devenport, and D. J. Cohen, Overriding native cell coordination enhances external programming of collective cell migration, *Proc. Natl. Acad. Sci. USA* **118**, e2101352118 (2021).
- [45] A. Puliafito, L. Hufnagel, P. Neveu, S. Streichan, A. Sigal, D. K. Fygenson, and B. I. Shraiman, Collective and single cell behavior in epithelial contact inhibition, *Proc. Natl. Acad. Sci. USA* **109**, 739 (2012).
- [46] S. J. Streichan, C. R. Hoerner, T. Schneidt, D. Holzer, and L. Hufnagel, Spatial constraints control cell proliferation in tissues, *Proc. Natl. Acad. Sci. USA* **111**, 5586 (2014).
- [47] J. Yu, P. Cai, X. Zhang, T. Zhao, L. Liang, S. Zhang, H. Liu, and X. Chen, Spatiotemporal oscillation in confined epithelial motion upon fluid-to-solid transition, *ACS Nano* **15**, 7618 (2021).
- [48] L. Hufnagel, A. A. Teleman, H. Rouault, S. M. Cohen, and B. I. Shraiman, On the mechanism of wing size determination in fly development, *Proc. Natl. Acad. Sci. USA* **104**, 3835 (2007).
- [49] R. Farhadifar, J.-C. Röper, B. Aigouy, S. Eaton, and F. Jülicher, The influence of cell mechanics, cell-cell interactions, and proliferation on epithelial packing, *Curr. Biol.* **17**, 2095 (2007).
- [50] D. Bi, J. Lopez, J. M. Schwarz, and M. L. Manning, A density-independent rigidity transition in biological tissues, *Nat. Phys.* **11**, 1074 (2015).
- [51] D. Bi, X. Yang, M. C. Marchetti, and M. L. Manning, Motility-Driven Glass and Jamming Transitions in Biological Tissues, *Phys. Rev. X* **6**, 021011 (2016).
- [52] N. Noll, M. Mani, I. Heemskerk, S. J. Streichan, and B. I. Shraiman, Active tension network model suggests an exotic mechanical state realized in epithelial tissues, *Nat. Phys.* **13**, 1221 (2017).
- [53] K. K. Chiou, L. Hufnagel, and B. I. Shraiman, Mechanical stress inference for two-dimensional cell arrays, *PLoS Comput. Biol.* **8**, e1002512 (2012).
- [54] G. W. Brodland, J. H. Veldhuis, S. Kim, M. Perrone, D. Mashburn, and M. S. Hutson, Cellfit: A cellular force-inference toolkit using curvilinear cell boundaries, *PLoS One* **9**, e99116 (2014).
- [55] R. Vasan, M. M. Maleckar, C. D. Williams, and P. Rangamani, Dlite uses cell-cell interface movement to better infer cell-cell tensions, *Biophys. J.* **117**, 1714 (2019).
- [56] C. Roffay, C. J. Chan, B. Guirao, T. Hiiragi, and F. Graner, Inferring cell junction tension and pressure from cell geometry, *Development* **148**, dev192773 (2021).
- [57] V. Nier, G. Peyret, J. d'Alessandro, S. Ishihara, B. Ladoux, and P. Marcq, Kalman inversion stress microscopy, *Biophys. J.* **115**, 1808 (2018).
- [58] K. Aoki, Y. Kumagai, A. Sakurai, N. Komatsu, Y. Fujita, C. Shionyu, and M. Matsuda, Stochastic ERK activation induced by noise and cell-to-cell propagation regulates cell density-dependent proliferation, *Mol. Cell* **52**, 529 (2013).

- [59] M. H. Köpf and L. M. Pismen, A continuum model of epithelial spreading, *Soft Matter* **9**, 3727 (2013).
- [60] S. Henkes, Y. Fily, and M. C. Marchetti, Active jamming: Self-propelled soft particles at high density, *Phys. Rev. E* **84**, 040301(R) (2011).
- [61] M. Basan, J. Elgeti, E. Hannezo, W.-J. Rappel, and H. Levine, Alignment of cellular motility forces with tissue flow as a mechanism for efficient wound healing, *Proc. Natl. Acad. Sci. USA* **110**, 2452 (2013).
- [62] J. M. López-Gay, H. Nunley, M. Spencer, F. di Pietro, B. Guirao, F. Bosveld, O. Markova, I. Gaugue, S. Pelletier, D. K. Lubensky, and Y. Bellaïche, Apical stress fibers enable a scaling between cell mechanical response and area in epithelial tissue, *Science* **370**, eabb2169 (2020).
- [63] A. Shellard and R. Mayor, Supracellular migration—Beyond collective cell migration, *J. Cell Sci.* **132**, jcs226142 (2019).
- [64] X. Wang, M. Merkel, L. B. Sutter, G. Erdemci-Tandogan, M. L. Manning, and K. E. Kasza, Anisotropy links cell shapes to tissue flow during convergent extension, *Proc. Natl. Acad. Sci. USA* **117**, 13541 (2020).
- [65] H. G. Yevick, P. W. Miller, J. Dunkel, and A. C. Martin, Structural redundancy in supracellular actomyosin networks enables robust tissue folding, *Dev. Cell* **50**, 586 (2019).
- [66] A. S. Eritano, C. L. Bromley, A. B. Albero, L. Schütz, F.-L. Wen, M. Takeda, T. Fukaya, M. M. Sami, T. Shibata, S. Lemke *et al.*, Tissue-scale mechanical coupling reduces morphogenetic noise to ensure precision during epithelial folding, *Dev. Cell* **53**, 212 (2020).
- [67] S. Xie and A. C. Martin, Intracellular signalling and intercellular coupling coordinate heterogeneous contractile events to facilitate tissue folding, *Nat. Commun.* **6**, 7161 (2015).